# ATLAS-FREE BRAIN SEGMENTATION IN 3D PROTON-DENSITY-LIKE MRI IMAGES

*Daniel Schmitter*[1]*, Ricard Delgado-Gonzalo*[1]*, Gunnar Krueger*[2]*, and Michael Unser* [1]

[1]Biomedical Imaging Group, École polytechnique fédérale de Lausanne (EPFL), Switzerland
[2]Advanced Clinical Imaging Technology Group, Siemens Healthcare Sector, Renens, Switzerland

## ABSTRACT

We present a new method for the atlas-free brain segmentation of proton-density-like 3D MRI images. We show how steerable filters can be efficiently combined with parametric spline surfaces to produce a fast and robust 3D brain segmentation algorithm. The novelty lies in the computation of brain edge maps through optimal steerable surface detectors which provide efficient energies for the rapid optimization of snakes. Our experimental results show the promising potential of the method for fast and accurate brain extraction.

***Index Terms***— brain segmentation, steerable filter, spline snake, atlas-free, active contours.

## 1. INTRODUCTION

Brain-segmentation algorithms are extensively used to examine disease-related structural and morphological changes that occur in the brain. Such methods tend to be computationally expensive because 3D volumes need to be processed. Most of the algorithms rely on atlas-based registration methods, which make the overall algorithm computationally expensive [1, 2]. Furthermore, they might bias the outcome if either the patient scan or the registration algorithm do not match the template image well [3].

Active contours and surfaces (a.k.a. snakes) provide an alternative to atlas-based segmentation. They have been widely used to segment simple biomedical structures in 2D [4, 5]. However, snakes often require user interaction, which makes them less suitable for 3D medical imaging. We propose to make use of a 3D parametric spline snake for the atlas-free segmentation of the brain surface. Its parameterization allows us to implement a fast algorithm that has been proven to be competitive with the state of the art [6]. The segmentation is formulated as an energy-minimization problem [7]. Defining an efficient energy function is crucial for fast segmentation because it determines the speed of the optimization process as well as the accuracy of the result. In 3D, edge maps provide a convenient way to compute energy terms because they allow one to bypass the expensive evaluation of volume integrals at each iteration by replacing them by surface-based terms [6]. We show how steerable filters [8] combined with Canny-like criteria [9] can be used to compute edge maps through the implementation of optimal 3D steerable surface detectors [10, 11, 12]. We have tested the efficiency of our proposed framework of steerable filters and parametric spline snakes for brain segmentation on realistic brain phantoms [13] and show its capability to be fast and robust.

This work was funded in part by the Swiss SystemsX.ch initiative under Grant 2008/005, the Swiss National Science Foundation under Grant 200020-144355, the Center for Biomedical Imaging of the Geneva-Lausanne Universities and EPFL, as well as by the Foundations Leenaards and Louis-Jeannet.

## 2. FEATURE DETECTION WITH 3D STEERABLE FILTERS

To compute the 3D edge maps we make use of steerable filters. They were first introduced in [8] as a family of filters that can be efficiently rotated by representing them through a linear combination of appropriate basis filters. Therefore, steerable filters provide a convenient framework for rotation-invariant feature detection. We use $M$th order steerable derivative-based filters whose impulse response takes the form

$$h(\boldsymbol{x}) = \sum_{m=1}^{M} \sum_{n=0}^{m} \sum_{p=0}^{m-n} \alpha_{m,n,p} \underbrace{\frac{\partial^n}{\partial x^n} \frac{\partial^p}{\partial y^p} \frac{\partial^{m-n-p}}{\partial z^{m-n-p}} g(\boldsymbol{x})}_{h_{m,n,p}(\boldsymbol{x})}$$

where $g$ is an isotropic 3D Gaussian function and $\alpha_{m,n,p}$ are the weights of the basis functions. In this paper, we use $\boldsymbol{x}$ to describe a point $(x, y, z)$ in 3D space.

Defining the rotation matrix $\boldsymbol{R}_{\theta,\phi}$, a feature with a particular orientation located in 3D space can be detected by a rotated version of the feature template $h(-\boldsymbol{x})$ through estimation of its Euler angles by

$$(\theta^*(\boldsymbol{x}), \phi^*(\boldsymbol{x})) = \underset{\theta,\phi}{\operatorname{argmax}} (f(\boldsymbol{x}) * h(\boldsymbol{R}_{\theta,\phi}\boldsymbol{x})).$$

The response of the filter to an image $f$ is given by

$$r^*(\boldsymbol{x}) = f(\boldsymbol{x}) * h(\boldsymbol{R}_{\theta*,\phi*}\boldsymbol{x}).$$

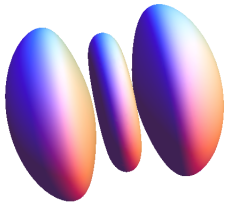

**Fig. 1**. Isosurface representation of the optimal surface detector.

### 2.1. Designing the Optimal Surface Detector

The generalized optimality criterion to derive a feature detector was originally proposed in 2D in [10] and extended to 3D in [11]. We use it to derive an optimal 2nd-order surface detector. We choose $f_0(\boldsymbol{x}) = \delta(x)$ as our idealized surface template, where $\delta$ denotes the Dirac delta. The response of the filter to the surface template centered at the origin is given by

$$S = (f_0 * h)(\mathbf{0}) = \int_{\mathbb{R}^3} f_0(\boldsymbol{x}) h(-\boldsymbol{x}) \mathrm{d}\boldsymbol{x}.$$

The localization error (due to the presence of noise) in the direction orthogonal to the surface is quantified by

$$Loc = -\int_{\mathbb{R}^3} f_0(\boldsymbol{x}) \frac{\partial^2}{\partial x^2} h(-\boldsymbol{x}) \mathrm{d}\boldsymbol{x}.$$

We maximize $(S \cdot Loc)$ using Lagrangian optimization, while imposing unit energy on the filter as $\int_{\mathbb{R}^3} |h(\boldsymbol{x})|^2 \mathrm{d}\boldsymbol{x} = 1$.

This yields the optimal surface detector

$$h(\boldsymbol{x}) = \frac{\sigma}{8\pi\sqrt{3}} (\Delta g(\|\boldsymbol{x}\|) - 5 g_{xx}(\boldsymbol{x})) \qquad (1)$$

where $\Delta$ denotes the Laplacian operator, $\sigma$ is the standard deviation of the Gaussian and $g_{xx} = \frac{\partial^2 g}{\partial x^2}$. An isosurface representation of (1) is shown in Figure 1.

### 2.2. Surface Detection

To express the rotated version of (1), we make use of the property $\mathcal{D}_v^2 f = \boldsymbol{v}^T \boldsymbol{H}_f \boldsymbol{v}$, where $\mathcal{D}_v$ denotes the operator describing the directional derivative, $\boldsymbol{H}_f$ is the 3D Hessian matrix of $f$, and $\boldsymbol{v} = (\cos\theta \sin\phi, \sin\theta \sin\phi, \cos\phi)$ is a unit vector specifying an arbitrary orientation in 3D. Thus, $h(\boldsymbol{R}_{\theta,\phi}\boldsymbol{x}) \propto \Delta g(\|\boldsymbol{x}\|) - 5\boldsymbol{v}^T \boldsymbol{H}_g(\boldsymbol{x}) \boldsymbol{v} = \boldsymbol{\beta}_g(\boldsymbol{x})$ and

$$(f * h(\boldsymbol{R}_{\theta,\phi} \cdot))(\boldsymbol{x}) \propto \boldsymbol{v}^T \boldsymbol{\beta}_{f*g}(\boldsymbol{x}) \boldsymbol{v}. \qquad (2)$$

Applying the constraint $\boldsymbol{v}^T \boldsymbol{v} = 1$ on the unit vector $\boldsymbol{v}$ and maximizing (2), we obtain $\boldsymbol{\beta}_{f*g} \boldsymbol{v} = \lambda \boldsymbol{v}$. The optimal orientation is given by the eigenvector $\boldsymbol{v}_{max}$ corresponding to the largest eigenvalue $\lambda_{max}$ of $\boldsymbol{\beta}_{f*g}$, which also yields the maximum response of the detector. The result of the surface detection is shown in Figure 2 (top right).

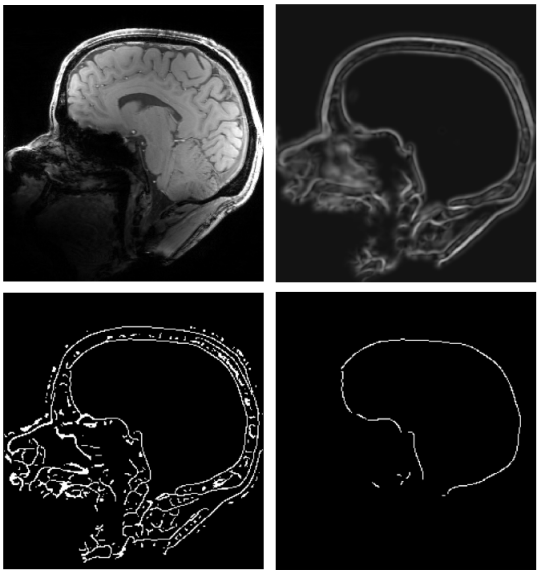

**Fig. 2**. 2D sagittal cross section of the detected 3D surface. Top row: Original proton-density image (left) and result of steerable filtering (right). Bottom row: Result of NMS and thresholding (left) and extracted largest component (right).

### 2.3. Surface Refinement

In order to better delineate the surface, a classical non-maximum suppression (NMS) in the direction orthogonal to the surface is applied followed by a thresholding step in order to obtain a binary image (Figure 2, bottom right). The direction orthogonal to the surface is given by $\boldsymbol{v}_{max}$ described above. In Figure 2 (bottom left) we see that the brain appears as the innermost surface and is almost closed. To ensure additional robustness, we extract this inner surface before segmenting it. For this purpose we roughly estimate the center of the brain. Then, we iterate over all foreground voxels, and keep only the ones closest to the center (in the direction orthogonal to the surface). Among the retained voxels we extract the largest component, whose 2D representation is shown in Figure 2 (bottom right).

## 3. 3D PARAMETRIC SPLINE SNAKE

We use the continuously defined 3D spline snake proposed in [6] to segment the extracted brain surface. It is a parametric surface whose expression is

$$\boldsymbol{\sigma}(u,v) = \sum_{i=0}^{M_1-1} \sum_{j=-1}^{M_2+1} \boldsymbol{c}[i,j] \phi_{1,per}(M_1 u - i) \phi_2(M_2 v - j) \qquad (3)$$

where $\phi_{1,per}(u) = \sum_{n=-\infty}^{\infty} \phi_1(u - M_1 n), \forall u \in \mathbb{R}$, and $\boldsymbol{c}[i,j] \in \mathbb{R}^3$ are the control points in 3D. In (3), the basis

functions $\phi$ are made of exponential B-splines and are defined as

$$\phi_1(u) = \begin{cases} \frac{\cos\left(\frac{2\pi|u|}{M_1}\right)\cos\left(\frac{\pi}{M_1}\right)-\cos\left(\frac{2\pi}{M_1}\right)}{1-\cos\left(\frac{2\pi}{M_1}\right)} & 0 \leqslant |u| < \frac{1}{2} \\ \frac{1-\cos\left(\frac{2\pi(3/2-|u|)}{M_1}\right)}{2\left(1-\cos\left(\frac{2\pi}{M_1}\right)\right)} & \frac{1}{2} \leqslant |u| < \frac{3}{2} \\ 0 & \frac{3}{2} \leqslant |u| \end{cases}$$

$$\phi_2(v) = \begin{cases} \frac{\cos\left(\frac{\pi|v|}{M_2}\right)\cos\left(\frac{\pi}{2M_2}\right)-\cos\left(\frac{\pi}{M_2}\right)}{1-\cos\left(\frac{\pi}{M_2}\right)} & 0 \leqslant |v| < \frac{1}{2} \\ \frac{1-\cos\left(\frac{\pi(3/2-|v|)}{M_2}\right)}{2\left(1-\cos\left(\frac{\pi}{M_2}\right)\right)} & \frac{1}{2} \leqslant |v| < \frac{3}{2} \\ 0 & \frac{3}{2} \leqslant |v|. \end{cases}$$

Considering additional conditions on the poles of the surface, a total of $M_1(M_2-1)+4$ control points are necessary to define the snake in a continuous way. Due to its spline-based structure, the snake surface can adopt the shape of any kind of closed surface with arbitrary precision.

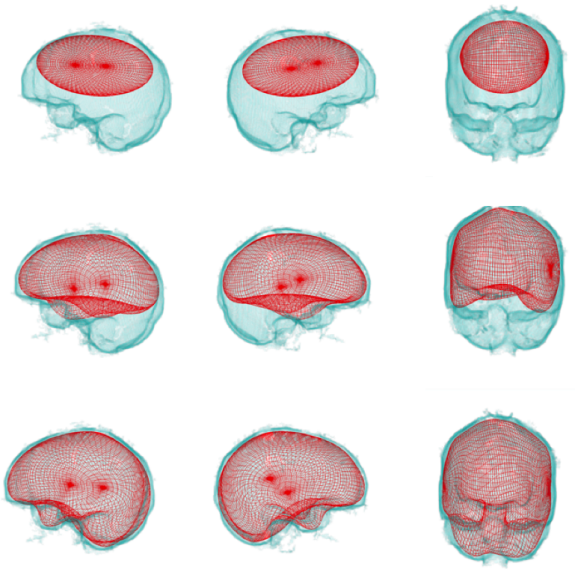

**Fig. 3**. Wireframe representation of the parametric surface. The 3D spline snake is initialized as an ellipsoid (top row). Through minimization of the energy term (4), it segments the brain surface (middle row). The final segmentation result is shown in the bottom row.

### 3.1. Fast Optimization

The segmentation process is formulated as an energy-minimization problem. The refined surface image (Figure 2, bottom right) provides an ideal edge map to guide the snake towards the desired boundary. We use it to calculate the gradient energy proposed in [6], which is defined as

$$\begin{aligned} E_{grad} &= -\oiint_S \boldsymbol{\nabla} f \cdot \mathrm{d}\boldsymbol{S} = -\oiint_S \left(\boldsymbol{\nabla} f \cdot \frac{\boldsymbol{n}}{\|\boldsymbol{n}\|}\right) \mathrm{d}S \\ &= -\iiint_V \mathrm{div}(\boldsymbol{\nabla} f)\mathrm{d}V = \iiint_V -\Delta f \mathrm{d}V \\ &= -\oiint_{\partial V} (\Delta f)^x \mathrm{d}y \wedge \mathrm{d}z \end{aligned} \tag{4}$$

where $(\Delta f)^x = \int_{-\infty}^{x} \Delta f(\tau, y, z)\mathrm{d}\tau$ and $\wedge$ denotes the wedge product. In the last step of (4), Gauss' theorem has been used. The quantity $(\Delta f)^x$ can be precomputed and stored in a look-up table to allow fast energy computation. The optimization process is visualized in Figure 3.

### 3.2. Snake Initialization

We initialized the snake as an ellipsoid lying completely within the brain surface (Figure 3, top row). Therefore, during optimization, the snake will primarily expand rather than shrink.

## 4. EXPERIMENTS

We have validated our algorithm on the BrainWeb PD phantom [13], where the ground truth is known. Our method was tested with the original bias- and noise-free image, as well as with increasing radio-frequency (RF) intensity non-uniformities of 20% and 40% and increasing additive white Gaussian noise levels ranging from 1 to 9%. Measures of overlap between the segmented brain masks and the gold standard were calculated according to the Dice and Jaccard similarity indices. Additionally, the inter-subject variability was evaluated by computing similarity coefficients between the corrupted images and the bias- and noise-free image. The initial position of the surface snake was the same throughout the experiments. We used $M_1 = M_2 = 9$ to evaluate (3). Therefore, 76 control points were used. The experiments were run without user interaction.

### 4.1. Robustness, Accuracy, and Computational Aspects

The results of the measures of similarity are given in Table 1 and illustrated in Figure 4. The high degree of overlap with respect to the gold standard confirms the selectivity of the surface detector. Its capacity to detect surface elements is not hampered by bias or noise in the image. This is due to its property of being an optimal 'matched' detector. The measures for inter-subject variability are even higher and show additional robustness of the method with respect to different scanning conditions. Worsening the image quality did not sig-

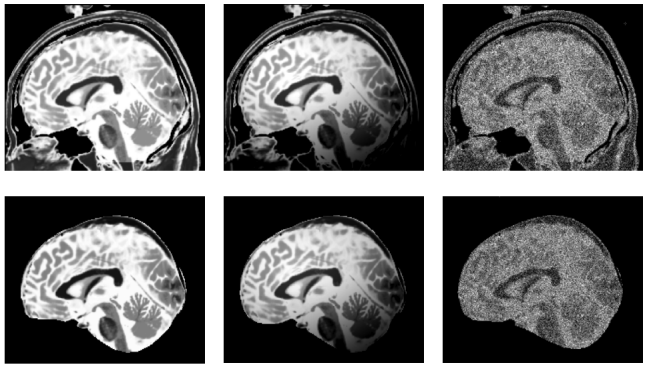

**Fig. 4**. 2D sagittal cross section of 3D simulated Brainweb data (top row) and the corresponding segmented images (bottom row). Left column: noise and bias free images; middle: biased images (40% RF intensity non-uniformity); right: noisy images (9% additive Gaussian white noise).

nificantly affect the final segmentation, which indicates the reproducibility of the method. Besides, the algorithm was also tested on 12 real subjects with a satisfying outcome (data not shown). Furthermore, our algorithm is fast enough to be run in a doctor-patient encounter. The implementation of our algorithm executes in less than 70 seconds on average on a standard computer (3.3 GHz, 16GB RAM).

| | gold standard | inter subject |
|---|---|---|
| Dice | $0.9522 \pm 0.0011$ | $0.9806 \pm 0.0047$ |
| Jaccard | $0.9087 \pm 0.0020$ | $0.9620 \pm 0.0090$ |

**Table 1**. Dice and Jaccard similarity coefficients.

## 5. CONCLUSIONS

We provide a new solution for fast brain segmentation in 3D MRI proton-density-like images. Our study shows how 3D parametric spline snakes can be used for this purpose. Our method relies on 3D edge maps which allow fast snake optimization through the computation of surface integrals, thereby avoiding tedious integration of volumes. Based on steerable filters, we show how an optimal surface detector can be used to compute such edge maps. We have demonstrated the robustness of the proposed method with respect to radio-frequency-induced intensity inhomogeneities, as well as noise. Our algorithm is fast and atlas-free. No user interaction is required. It therefore shows the potential to satisfy the requirements needed to be run in clinical routine.

## 6. REFERENCES


[1] J. Ashburner, "A fast diffeomorphic image registration algorithm," *NeuroImage*, vol. 38, no. 1, pp. 95–113, October 2007.

[2] A. M. Dale, B. Fischl, and M. I. Sereno, "Cortical surface-based analysis: I. Segmentation and surface reconstruction," *NeuroImage*, vol. 9, no. 2, pp. 179 – 194, February 1999.

[3] B. Moeller and S. Posch, "An integrated analysis concept for errors in image registration," *Pattern Recognition and Image Analysis*, vol. 18, no. 2, pp. 201–206, June 2008.

[4] C. Zimmer, E. Labruyere, V. Meas-Yedid, N. Guillen, and J.-C. Olivo-Marin, "Segmentation and tracking of migrating cells in videomicroscopy with parametric active contours: A tool for cell-based drug testing," *IEEE Trans. Medical Imaging*, vol. 21, no. 10, pp. 1212–1221, October 2002.

[5] Y.-L. Fok, J. C. K. Chan, and R.T. Chin, "Automated analysis of nerve-cell images using active contour models," *IEEE Trans. Medical Imaging*, vol. 15, no. 3, pp. 353–368, June 1996.

[6] R. Delgado-Gonzalo, N. Chenouard, and M. Unser, "Spline-based deforming ellipsoids for interactive 3D bioimage segmentation," *IEEE Trans. Image Processing*, vol. 22, no. 10, pp. 3926–3940, October 2013.

[7] M. Kass, A. Witkin, and D. Terzopoulos, "Snakes: Active contour models," *International Journal of Computer Vision*, vol. 1, no. 4, pp. 321–331, January 1988.

[8] W. T. Freeman and E. H. Adelson, "The design and use of steerable filters," *IEEE Trans. Pattern Analysis and Machine Intelligence*, vol. 13, no. 9, pp. 891–906, September 1991.

[9] J. Canny, "A computational approach to edge detection," *IEEE Trans. Pattern Analysis and Machine Intelligence*, vol. 8, no. 6, pp. 679–698, November 1986.

[10] M. Jacob and M. Unser, "Design of steerable filters for feature detection using Canny-like criteria," *IEEE Trans. Pattern Analysis and Machine Intelligence*, vol. 26, no. 8, pp. 1007–1019, August 2004.

[11] F. Aguet, M. Jacob, and M. Unser, "Three-dimensional feature detection using optimal steerable filters," *Proceedings of the 2005 IEEE International Conference on Image Processing (ICIP'05)*, vol. II, pp. 1158–1161, 11.-14. September 2005.

[12] C. S. Seelamantula, F. Aguet, S. Romain, P. Thevenaz, and M. Unser, "Parametric B-spline snakes on distance maps—application to segmentation of histology images," *European Conference on Signal Processing 2008*, 2008.

[13] R.K.-S. Kwan, A.C. Evans, and G.B. Pike, "MRI simulation-based evaluation of image-processing and classification methods," *IEEE Trans. Medical Imaging*, vol. 18, no. 11, pp. 1085–1097, November 1999.